Biosensors and Bioelectronics: X 14 (2023) 100383

Contents lists available at ScienceDirect

Biosensors and Bioelectronics: X

journal homepage: www.journals.elsevier.com/biosensors-and-bioelectronics-x

An affordable automated LED array system for optimizing photodynamic therapy protocols

Andrea L. Larraga-Urdaz [a], Adrián Vizcaíno [b], Marta Valledor [b], Francisco Ferrero [b,*], Juan Carlos Campo [b], Alberto López [b], J.M. Costa-Fernández [a], María Luisa Fernández-Sánchez [a]

[a] Dept. of Physical and Analytical Chemistry, University of Oviedo, 33006, Oviedo, Spain
[b] Dept. of Electrical, Electronic, Communications, and Systems Engineering, University of Oviedo, Campus of Gijón, 33204, Gijón, Spain

ARTICLE INFO

Keywords:
Theragnostic
Photodynamic therapy
Photosensitizer
Lighting protocols
Cell viability
Reactive oxygen species

ABSTRACT

Photodynamic therapy (PDT) is a promising minimally invasive alternative cancer treatment that, due to fluorescent properties of the drug (photosensitizer), can be used as a theragnostic agent. The efficacy of this treatment largely relies on the successful activation of the photosensitizer with appropriate light. While certain studies demonstrate comparable outcomes between LED and laser activation, there remains a lack of consensus regarding the differential effects of pulsed versus continuous light. In response to the limited availability of commercially versatile equipment capable of fully controlling pulsed light, we have developed an LED array system for optimizing PDT protocols. The designed equipment is versatile, has an intuitive user-friendly interface, and adapts to sterile conditions required for in-vitro studies. It also enables precise control of light irradiation, allowing to freely modify power, pulse width, frequency, exposure time and wavelength. In this study, the developed LED array system was employed to optimize PDT protocols for breast cancer theragnostic, using Fotoenticine as photosensitizer. The obtained results highlight the importance of appropriate irradiation equipment in PDT lighting protocol optimization. In this sense, significant improvements in therapeutic efficacy were observed when using 10 Hz frequency and 10 or 20% duty cycles. This resulted in a remarkable transition from a non-cytotoxic dose in continuous mode to a fully cytotoxic condition, leading to a >95% enhancement in the therapeutic effect.

1. Introduction

Nowadays, the most common cancer treatments are still chemotherapy and radiotherapy. However, these treatments affect the surrounding healthy cells and produce serious side effects. Photodynamic therapy (PDT) is emerging as a promising alternative treatment that selectively damages tumour cells, minimizing treatment-related side effects (Yanovsky et al., 2019; Kercher et al., 2020; Agostinis et al., 2011; Robertson et al., 2009; Ogawa and Kobuke, 2008; Calixto et al., 2016). Moreover, PDT induces a different cell death mechanism than chemotherapy and is even effective for the treatment of chemoresistant cells (Cramer et al., 2020). Currently, PDT presents a localized and controllable approach applicable to a broad range of diseases, including infectious disorders and several types of cancer (Pereira et al., 2013).

PDT is a light-based treatment method that involves the administration of a photosensitizer (PS) to the target tissue, followed by its activation through irradiation with light of an appropriate wavelength. This activation process triggers the production of reactive oxygen species (ROS), causing extensive damage inside cell structures (Zhang et al., 2022; Chudy et al. 2018; Kwiatkowski et al., 2018; Correia et al., 2021). Furthermore, the PS fluorescence characteristics can be employed for the clinical visualization of a tumour, facilitating precise delimitation of the irradiation area and, consequently, functioning as theragnostic agent. Simultaneously serving as diagnosis imaging tools and therapeutic agent upon light activation.

Different light-delivery approaches for PDT have been developed for different indications and scenarios. These include mainly laser sources and non-laser sources such as light-emitting diodes (LEDs). Laser sources are the most widely used due to their high intensity, coherence, and directionality. This allows suitable light to be targeted precisely to the target area. Nevertheless, they produce monochromatic light, which limits the number of PSs that can be used since each presents a slightly different activation wavelength (Yoon et al., 2013; Kim and Darafsheh, 2020). Recently, through the development of new-generation LEDs, PS

* Corresponding author.
E-mail address: ferrero@uniovi.es (F. Ferrero).

https://doi.org/10.1016/j.biosx.2023.100383
Received 16 May 2023; Received in revised form 10 July 2023; Accepted 13 July 2023
Available online 16 July 2023

activation has also been accomplished. These LEDs present increased power output, a variety of emission wavelengths and different emission bandwidths. These features, combined with the low cost and easy modulation of these materials, makes these LEDs a viable and appealing alternative to traditional medical laser sources for PDT applications (Kirino et al., 2020; Jiang et al., 2015; Sailapu et al., 2019; Liu et al., 2019; Hempstead et al. 2015).

Another factor that plays a crucial role in determining the effectiveness of treatment is the irradiation parameters. Through modulation of the frequency, pulse width and power, pulsed light similar to continuous light is achieved. Although previous studies have clearly shown comparable drug activation efficiencies between LEDs and laser sources, highlighting the portability and low-cost of LED-based devices (Lin et al., 2010; Zeitouni et al., 2014; de Figueiredo et al., 2017; Yu et al., 2009; Zhang et al., 2017), there has been no consensus on the effects of pulsed and continuous light. Although some evidence has shown that pulsed light may help tissues/cells reoxygenate and prevent a high thermal response, the results have been contradictory (Davanzo et al., 2017; Klimenko et al., 2016; Chen et al., 2016; Yuzhakova et al., 2021; Turna et al., 2022). It is also important to note that most devices used to study pulsed light parameters don't allow complete control of the pulse parameters, sometimes limiting the studies to one type of pulse. This clearly demonstrates the limitations of commercially available devices. The development of better equipment with more features for PDT studies is still underway (Sailapu et al., 2019; Liu et al., 2019). To the best of our knowledge, very few devices meet the requirements for full and precise pulsed light control while satisfying the required standards for in vitro studies carried out in ELISA well plates under strict sterile conditions. In this article, to the best of our knowledge, we present a uniquely portable and cost-effective wireless device able to modify the irradiation wavelength, power, duty, frequency, and exposure time, allowing us to fully study the effect of the light parameters of multiple PSs and, therefore, fully aiding the design of an optimum irradiation protocol to achieve outstanding photoactivation efficacy.

The device was designed for the irradiation of a 96-well ELISA well plate, is easily sterilizable, practical for working under laminar flow hoods and provides total control not only of the light pulse but also of the wavelength by using a series of interchangeable LEDs. Additionally, it is an affordable wireless device controlled through a user-friendly web page from which irradiation protocols can be controlled and programmed, enabling telemedicine applications.

This equipment has been applied to examine the impact of pulsed and continuous light parameters on the effectiveness of the PS Fotoenticine® in the PDT of breast cancer cells as it guarantees comprehensive control over the irradiation parameters. Despite testing only one photosensitizer, the device's features enable its application to a wide variety of photosensitizers. The results indicate that employing pulsed irradiation with the same energy as continuous mode yields superior therapeutic effects.

2. Materials and methods

2.1. Reagents

The PS Fotoenticine® derived from Chlorin e6 was provided by the Spanish company Nuevas Tecnologías Científicas. Surfactant Triton-X-100, Dulbecco's modified Eagle's medium (DMEM) – high glucose, Dulbecco's phosphate-buffered saline (PBS), antibiotic antimycotic solution for cell culture, sodium pyruvate powder for cell culture and MEM nonessential amino acid solution were purchased from Sigma Aldrich. Any additional reagents and materials used during this article are named in the supplementary information.

2.2. Cell culture

The cell lines MDA-MB-231 and MCF-7 were acquired from the cell bank of Scientific and Technical Services, Oviedo (Spain), and fibroblasts from healthy mammoplasty tissue were acquired at the cell bank of the Hospital Foundation Jove. All the cell lines were cultured in DMEM supplemented with 10% bovine foetal serum and 1% penicillin/streptomycin solution. The fibroblast culture medium was supplemented with a nonessential amino acid solution without L-glutamine. The cells were maintained in a controlled environment of 37°C, 65% relative humidity and 5% CO_2 in an incubator. For cell counting, a commercial disposable hemocytometer FAST READ 102® was used.

2.3. Fotoenticine® cytotoxicity

PS cytotoxicity was assessed using a commercially available WST-1 kit from Roche. MDA-MB-231 cells were seeded at a density of 10^4 cells/well in 96-well plates and cultured for 24 h. Following cells adhesion, the cells were exposed to different concentrations of Fotoenticine® (5-50 ppm) for different duration (40 and 60 min). After the incubation period, the cells were washed twice with 200 μL of PBS, and a mixture of 100 μL of complete fresh medium and 10 μL of WST-1 reagent was added and incubated for 4 h. Cell viability (Eq. (1)) was calculated as a percentage of the absorbance of treated cells relative to that of untreated cells (F1) and represented as the mean of triplicates ± standard deviation.

$$\%\ viability = \frac{Abs.\ treated\ cells - Background\ Abs.}{Abs.\ non\ treated\ cells - Background\ Abs.}\ x\ 100 \quad (1)$$

2.4. PS cellular internalization

To evaluate the selective accumulation of the PS in in cancer cells compared to healthy cells, two breast cancer cell lines (MDA-MB-231 and MCF7) and fibroblasts from healthy mammoplasty tissue were used. A density of 10^5 cells/well was incubated in a 12-well ELISA plate overnight at growing conditions. Following, the cell culture medium was replaced by fresh medium containing varying concentrations of the PS (5 and 7.5 ppm) and incubated for 1 or 24 h. Afterwards, the cells were detached with 500 μL of 10 mM EDTA for 10 min. The samples were measured with a Cytoflex S - Beckman Coulter cytometer using the violet diode excitation laser (405 nm).

The PS fluorescence signal (F) was measured with a violet-660-A detector. Cells without treatment were used to determine the basal fluorescence and settle the fluorescence threshold (F_0). The mean fluorescence intensity (n=3) was determined, and the results were expressed as a ratio (F/F_0).

2.5. Confocal microscopy

Cancer cell lines (MDA-MB-231 and MCF-7) were seeded in a 24-well ELISA plate containing treated coverslips at a density 3.5×10^4 cells/well and incubated overnight at 37 °C, in 5% CO_2 with 65% RH. Then, the cells were incubated with different PS concentrations (10 to 50 ppm) for 20 min. After incubation, the cells were washed with PBS and then fixed at room temperature for 12 min with a solution of 4% paraformaldehyde. Cells were washed extensively with PBS and stored in fresh PBS (500 μL). The cells were visualized with a Leica TCS-SP8X spectral confocal microscope. All confocal images were acquired using the same imaging settings.

2.6. Irradiation protocol

To assess how light parameters affect the drug activation efficiency, 10^4 cells/well were seeded in a 96-well ELISA plate for 24 h prior to the incubation of 25 ppm PS during 1 h. Afterwards, PS was washed, and fresh complete medium was added before proceeding with the irradiation protocols. To avoid any type of contamination, the LED equipment was sterilized inside a laminar flow hood for 15 min with UV light before

performing any experiments. Initially, irradiation protocols in continuous mode with 660 and 810 nm LEDs were studied, followed by those in pulsed mode. The wavelengths were selected considering the spectral characterization of Fotoenticine (see Fig. S1). The effectiveness of the irradiation protocols was evaluated by WST-1 assay. To compare the different pulsed modes, the total energy (E) and power (0.1W) remained constant (see Fig. 1). As the duty cycle is expressed as the percentage of time the light is ON, a duty cycle of 100% indicates continuous mode and 50% duty means the light is ON only half of the total assay time, regardless of the frequency.

3. Electronic prototype

To evaluate the effect of light protocol on PS activation during TDP, the light irradiation device was design to be able to switch from continuous to pulsed light just by changing the duty. In continuous mode, only the radiated power is controlled by varying the LED current, maintaining a homogeneous light distribution throughout the test. Pulsed mode allows variable radiated power, duty, and frequency allowing different energy distributions. Fig. 2 shows a block diagram of the electronic prototype designed for photodynamic therapies. The complete electronic schematic and mechanical assembly are provided in the supplementary information (Figs. S2–4).

3.1. Hardware design

Cells assays were conducted in a 96-well ELISA plate, arranged in a 12 × 8 array. To measure the fluorescence effectively, edge wells were not used (Fig. S5a). Due to the high cost of making an array of 60 LEDs, it was decided to use an array of only 6 LEDs instead (Fig. S5b) and move the array along the plate using a stepper motor. In this way, the number of drivers and control signals and the prototype cost were reduced, and a better control of the light emission was achieved. Considering the distance of only 1.5 mm between the LEDs and the wells, no interference in adjacent wells was observed (see Fig. S5c). On the other hand, dark well plates were used. They are recommended for fluorescence measurements due to their minimal backscattered light and low background fluorescence. Additionally, dark walls minimize inter-well crosstalk and autofluorescence.

The stepper motor used to move the LED array was a NEMA 17 from Schneider, powered by +12 V DC and controlled by a Pololu A4998 driver. This driver allows the motor to be controlled in a very simple way using two digital signals: a DIR signal determines the direction of rotation of the motor and a low-to-high transition on the STEP input sequences of the translator and advances the motor one increment. The screw accuracy is specified in the datasheet as 100 μm/300 mm. Because the distance between the wells is 9 mm, the error is ±3 μm. Along with the ten rows, this error accumulates. The maximum error is 30 μm in the 10^{th} column. This is a very low error rate. The combination of steeper motor and its driver also provides a motion precision of 10 μm/step ± 0.05 μm (2 mm screw pitch, 200 steps/rotation). However, these errors are not cumulative. One of the most remarkable features of stepper motors and its driver is their ability to position accurately (see Fig. S4d).

Because temperature and ageing impact LED emissions, two drivers were implemented to keep the LED optical power constant, as shown in Fig. S6. Each driver controls the current of three LEDs connected in series. TPS61165 drivers from Texas Instruments were used, which allow 1.2 A maximum output current. The drivers' electronic circuits were designed following the manufacturer's recommendations. To achieve a pulsed mode, a transistor was added in series with the LEDs, and a resistor was added in parallel with the transistor. A high-value resistor was chosen so that the current demand was not too high. Two pulse width modulation (PWM) signals were used to control each driver. PWM1 varies the output current (power), and PWM2 varies the frequency and duty cycle of the signal. The LED current was programmed externally using a current-sensing resistor in series with the LED string. The value of the current sense resistor (R_{SET}) was calculated by Eq. (2):

$$I_{LED} = \frac{V_{FB}}{R_{SET}} \tag{2}$$

where I_{LED} is the output current of the LEDs and V_{FB} is the regulated voltage of the feedback pin. The feedback voltage was regulated by a low

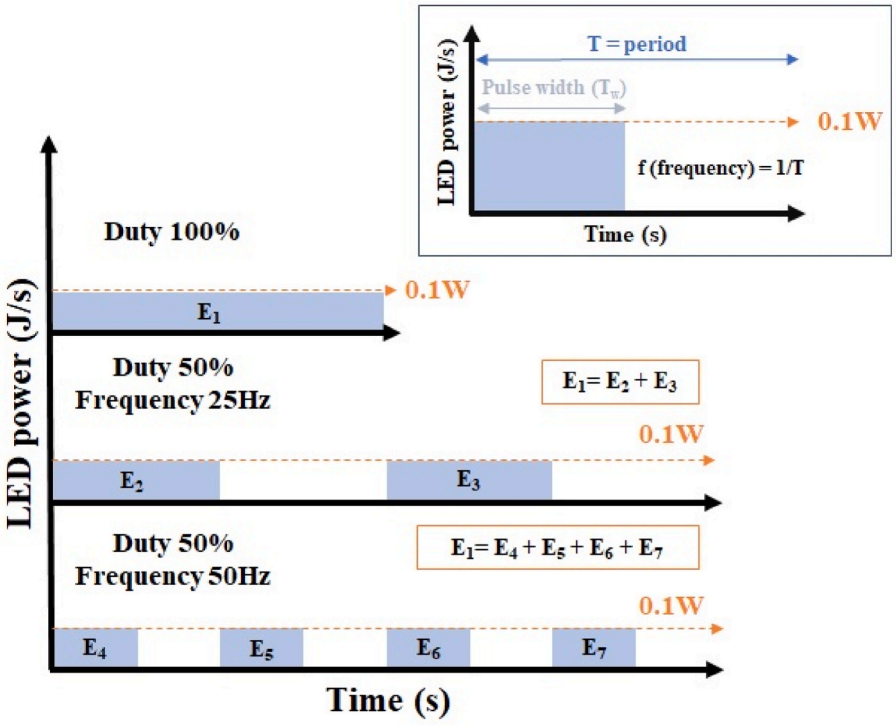

Fig. 1. Different pulsed light distribution according to the duty cycle and frequency conditions maintaining the total energy and irradiation power constant.

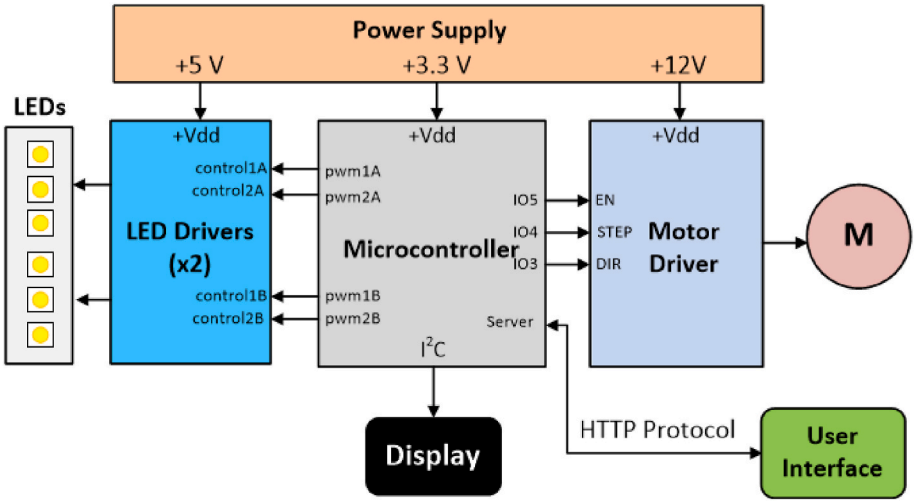

Fig. 2. Block diagram of the electronic prototype designed for photodynamic therapy.

0.2 V reference voltage. For a maximum LED current of 0.5 A, the R_{SET} was 0.4 Ω. To make the prototype more versatile for use with other LEDs, two resistors were added by a jumper. A value of 2 Ω resulted in a current of 100 mA for low-current LEDs, and a value of 0.25 Ω resulted in a current of 800 mA for high-current LEDs. As it was very important to develop a versatile system, LED modules that could be exchanged regardless of their wavelength, maximum current, forwards voltage, or other characteristics were used. In this prototype, two LED modules were designed, with wavelengths of 660 and 810 nm. The selected LEDs were LZ1-00R202 (660 nm, maximum current 1.2 A) and SST-10-IDR (810 nm, maximum current 1.5 A), from OSRAM LED Engin LuxiGen and LUMINUS, respectively.

To calibrate the equipment, it was necessary to determine the duty cycle that would provide the desired power level. This power varied between 0.1 W and the maximum power, with steps of 0.05 W. The datasheets of the LEDs give the relationship between the relative radiated power and the forwards current.

To perform the different tasks of the system, the ESP32 module from Espressif Systems was chosen. It includes a dual-core system with two CPUs. This module also integrates Wi-Fi and Bluetooth functionality through its SPI or I^2C interfaces. Engineered for mobile devices, wearable electronics, and Internet of Things (IoT) applications, ESP32 achieves ultralow power consumption with a combination of several types of proprietary software. ESP32 also includes state-of-the-art features, such as fine-grained clock gating, various power modes and dynamic power scaling. Although the user interface is based on a web page, a small screen (0.96'' OLED) and two LEDs (one green and one red) were incorporated into the frontal panel of the equipment, allowing the user to check the operating status.

3.2. Software design

The software was developed using the Arduino IDE in Microsoft Visual Studio Code. The programming language used was C++. Software development was based on object-oriented programming. The program's operation was divided into three tasks:

- Task 1: Process everything related to the web page. NodeMCU-32 is connected to a Wi-Fi network and serves the website at an IP address, managing all requests (GET/POST) from the client (Web page) to the server (NodeMCU).
- Task 2: Perform tests (activate the PWM signals that allow the drivers to operate) and update the red and green LED states.
- Task 3: Update the display and move the motor.

Wi-Fi can work in two modes. SoftAP mode (Fig. S7a) enables a software access point. It consists of creating a Wi-Fi local area server (WLAN) and configuring it through software as an access point. In this mode, a server set identifier (SSID) is activated that can be viewed from Wi-Fi client devices such as mobile devices and computers. In Station mode (Fig. S7b), the module is connected to a Wi-Fi network, working as a server. The ESP32 microcontroller serves the page at a fixed IP address. The Fig. S8 displays a screen operation flowchart. The web page was designed in HTML and CCS utilizing Bootstrap as the style library. JavaScript was used for website logic. In addition, AJAX was used to make asynchronous web pages, which are updated without reloading the page. The web page design is shown in the Fig. S9. On the right side of the web page, there are cards for each LED group. These cards allow the entry of parameters for the irradiation of samples at each position (frequency, time, duty, and power).

4. Experimental results and discussion

4.1. Fotoenticine® cellular internalization

The selective accumulation of Fotoenticine® in cancer cells (MDA-MB-231 or MCF-7) rather than in healthy fibroblasts was evaluated by flow cytometry. The results in Fig. 3 prove that under the same experimental conditions, cancer cells internalize a greater concentration of PS than healthy cells, even after 24 h of incubation, indicating the selective incorporation of PS into cancer cells.

To evaluate PS internalization in breast cancer cells (MCF-7 and MDA-MB-231), different concentrations of Fotoenticine (5-50 ppm) were incubated for various time intervals between 1 and 4 h. As expected, with longer exposure times and higher doses, more PS was accumulated inside both cancer cells lines (see Fig. S10).

Additionally, a confocal microscope was used to monitor MDA-MB-231 PS uptake, incubated at different concentration (10, 25 and 50 ppm) for 20 min (see Fig. 4). Consistent with the previous literature, the localization of Fotoenticine was observed within the cytoplasm (de Almeida et al., 2020). The Fotoenticine® fluorescence which falls close to the near-infrared windows facilitates its localization since cell autofluorescence and tissue scattering are reduced. This excitation wavelength also allows a greater penetration depth, making Fotoenticine® well-suited for in vivo imaging and diagnostic applications.

4.2. Effects of irradiation parameters on drug activation

Initially, Fotoenticine® cytotoxicity was evaluated at different concentrations (5-50 ppm) and times (40 and 60 min). None of the

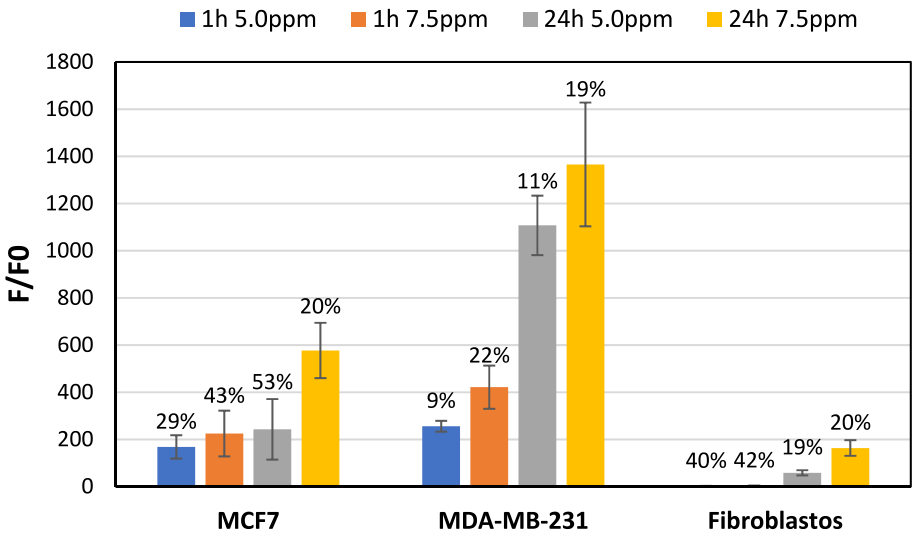

Fig. 3. Flow cytometry assay for the evaluation of the selective incorporation of PS in cancer cells and healthy fibroblasts. The relative standard deviations (RSDs) are in per cent.

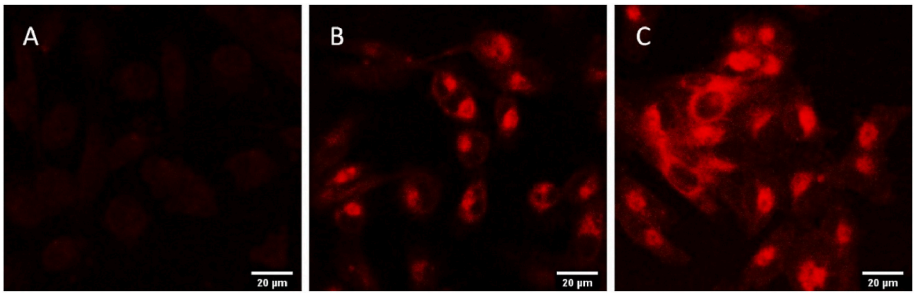

Fig. 4. Incorporation and localization of Fotoenticine® in MDA-MB-231 cells for 20 min with increasing concentrations. (a) 10 ppm. (b) 25 ppm. (c) 50 ppm. Scale bar, 20 µm.

conditions proved to be cytotoxic (see Fig. S11). For PDT studies, 25 ppm of PS and an incubation time of 1 h were selected for treating the MDA-MB-231 cells.

To assess the influence of light parameters (wavelength, power, frequency, and duty cycle), MDA-MB-231 treated with Fotoenticine® were submitted to different irradiation protocols using the developed LED-based illumination device. Initially, the effect of wavelength (660 and 810 nm) was evaluated in continuous mode. The irradiation power used in this case was 0.5 or 0.8 W for 10 min, resulting in a total energy application of 300 or 480 J, respectively. As shown in Fig. 5a, no cytotoxic effect was observed when 810 nm was used. Consequently, this wavelength was discarded for PS photoactivation. In contrast, LEDs at 660 nm effectively activated the drug, causing 60% cellular damage. Interestingly, it was observed that lower irradiation powers led to increased cell damage. This outcome can be attributed to the PS photosensitivity, as higher irradiation powers can cause degradation of the drug before its activation, reducing its effectiveness. Consequently, lower power (0.1 W) was employed for further studies of pulsed light effects where the roles that the duty cycle and frequency of the pulse play in the activation of the drug were evaluated.

As mentioned before, to compare different irradiation protocols, the irradiation power was fixed at 0.1 W, and the total energy irradiated was 60 J $\left(E = power\left(J/_S\right) \times T_{exposition}(s)\right)$. As shown in Fig. 5b, the most promising results were obtained when low duty cycles (10 and 20%) and frequencies (10 Hz) were applied, achieving cell death greater than 90%. However, duty cycles of 50% and frequencies of 50 and 80 Hz or continuous wavelength (CW) showed no significant effect. In these cases, the pulsed light was more similar to CW, as high frequencies and duty cycles were used. On the other hand, using low frequencies and duty cycles, small irradiation doses over a longer exposition time were applied, preventing PS photodegradation, allowing the cells to reoxygenate and therefore maintaining ROS production throughout the assay. In this way, viability below 5% were achieved when a frequency of 10 Hz and a duty cycle of 10 and 20% were applied.

The results of the present study agree with the existing literature, as it has been proven that pulsed light improves tissue/cells reoxygenate while minimizing excessive thermal response. This last effect enhances the PS stability which, in combination with a higher cellular oxygenation, leading to higher ROS production and greater cellular damage (Davanzo et al., 2017; Klimenko et al., 2016; Chen et al., 2016; Yuzhakova et al., 2021; Turna et al., 2022).

5. Conclusions

The low-cost LED array system has successfully fulfilled the requirements by facilitating a high-throughput and accurate optimization of irradiation protocols, thereby ensuring optimal performance of the photosensitizer. The continuous irradiation was performed at various wavelengths, confirming the effectiveness of 660 nm and ruling out the infrared wavelength for the photosensitizer activation. Additionally, a comparative analysis between pulsed and continuous light was conducted, demonstration a higher efficacy in activating the drug when short, spaced irradiation pulses were applied. Viabilities below 5% were achieve under low duty and frequencies conditions (10 or 20% and 10 Hz). Nevertheless, more research is needed to confirm if this rule holds true universally or if it depends on the cell line and photosensitizer being

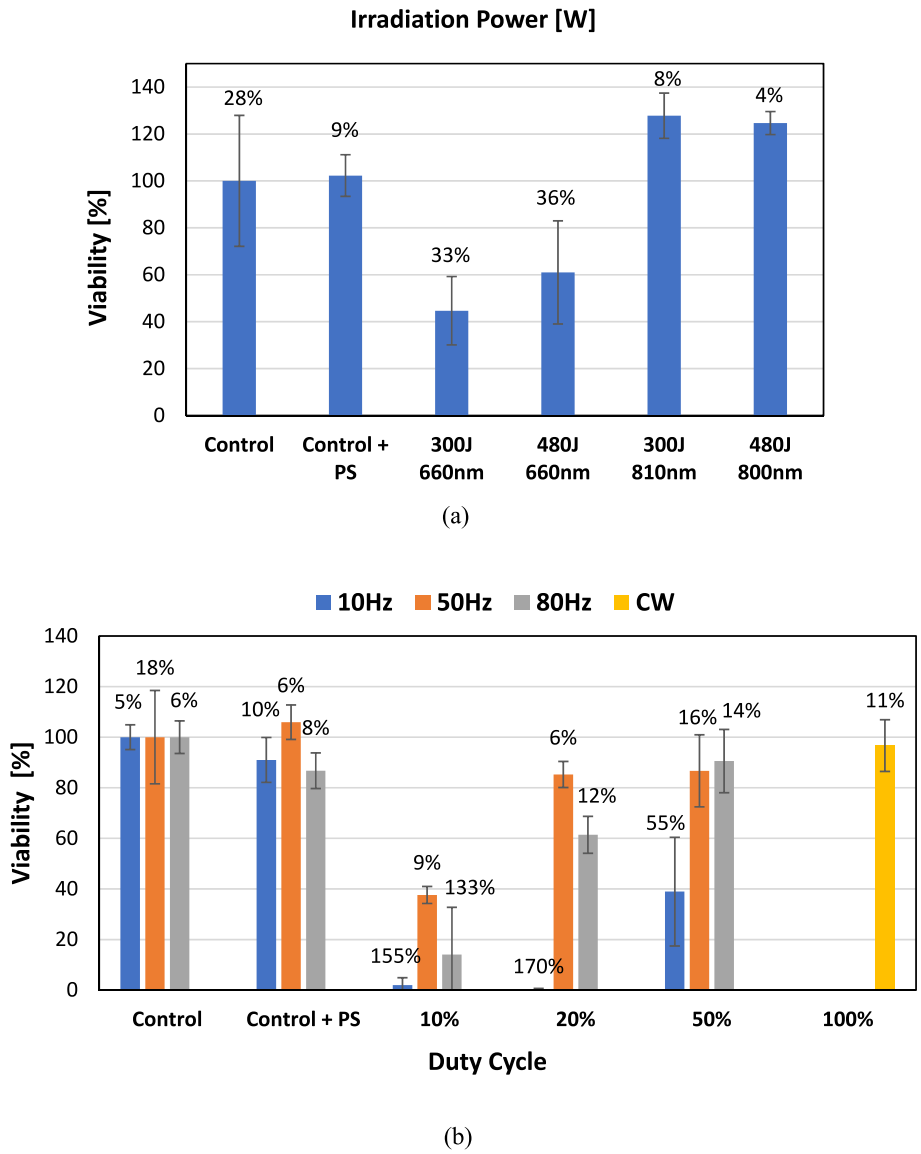

Fig. 5. Effect of the LEDs irradiation parameters on drug activation for MDA-MD-231 treatment. (a) Continuous mode at 660 and 810 nm. (b) Pulsed and continuous mode at 660 nm applying 60J. The relative standard deviations (RSDs) are in per cent.

used.

CRediT authorship contribution statement

Andrea L. Larraga-Urdaz: Conceptualization, Methodology, Validation, Writing – review & editing. **Adrián Vizcaíno:** Software. **Marta Valledor:** Writing and Editing. **Francisco Ferrero:** Writing – review & editing. **Juan Carlos Campo:** Software. **Alberto López:** Software. **J.M. Costa-Fernández:** Visualization, Supervision. **María Luisa Fernández-Sánchez:** Visualization, Supervision.

Declaration of competing interest

The authors declare that they have no known competing financial interests or personal relationships that could have appeared to influence the work reported in this paper.

Data availability

Data will be made available on request.

Acknowledgements

A.L.L.U acknowledges her PhD grant (BP19-059) from the Asturias Regional Government (Spain). This research was funded by the Spanish Ministry of Science and Innovation (PID2020-117282RB-I00 and MCI-20-PID2019-109698GB-I00) and by the Principado de Asturias AYUD/2021/51323.

Appendix A. Supplementary data

Supplementary data to this article can be found online at https://doi.org/10.1016/j.biosx.2023.100383.

References

Agostinis, P., Berg, K., Cengel, K.A., Foster, T.H., Girotti, A.W., Gollnick, S.O., Hahn, S. M., Hamblin, M.R., Juzeniene, A., Kessel, D., Korbelik, M., Moan, J., Mroz, P., Nowis, D., Piette, J., Wilson, B.C., Golab, J., 2011. Photodynamic therapy of cancer: an update. CA Cancer J Clin 61 (4), 250–281. https://doi.org/10.3322/caac.20114.

Calixto, G.M.F., Bernegossi, J., De Freitas, L.M., Fontana, C.R., Chorilli, M., 2016. Nanotechnology-based drug delivery systems for photodynamic therapy of cancer: a review. Molecules 21 (3), 342. https://doi.org/10.3390/molecules21030342.

Chen, D., Wang, Y., Li, B., Lin, H., Lin, X., Gu, Y., 2016. Effects of pulse width and repetition rate of pulsed laser on kinetics and production of singlet oxygen luminescence. J. Innov. Opt. Health Sci. 9 (6), 1650019 https://doi.org/10.1142/s179354581650019x.

Chudy, M., Tokarska, K., Jastrzębska, E., Bułka, M., Drozdek, S., Lamch, Ł., Wilk, K.A., Brzózka, Z., 2018. Lab-on-a-chip systems for photodynamic therapy investigations. Biosens. Bioelectron. 101, 37–51. https://doi.org/10.1016/j.bios.2017.10.013.

Correia, J.H., Rodrigues, J.A., Pimenta, S., Dong, T., Yang, Z., 2021. Photodynamic therapy review: principles, photosensitizers, applications, and future directions. Pharmaceutics 13 (9), 1332. https://doi.org/10.3390/pharmaceutics13091332.

Cramer, G.M., Moon, E.K., Cengel, K.A., Busch, T.M., 2020. Photodynamic therapy and immune checkpoint blockade. Photochem. Photobiol. 96, 954–961. https://doi.org/10.1111/php.13300.

Davanzo, N.N., Pellosi, D.S., Franchi, L.P., Tedesco, A.C., 2017. Light source is critical to induce glioblastoma cell death by photodynamic therapy using chloro-aluminiumphtalocyanine albumin-based nanoparticles. Photodiagnosis Photodyn. Ther. 19, 181–183. https://doi.org/10.1016/j.pdpdt.2017.04.017.

De Almeida, R.M.S., Fontana, L.C., dos Santos, G., Pereira, A.H.C., Soares, C.P., Pinto, J. G., Ferreira-Strixino, J., 2020. Analysis of the effect of photodynamic therapy with fotoenticine on gliosarcoma cells. Photodiagnosis Photodyn. Ther. 30, 1–11. https://doi.org/10.1016/j.pdpdt.2020.101685.

De Figueiredo, L.S., Rossoni, R.D., Jorge, A.O.C., Junqueira, J.C., 2017. Repeated applications of photodynamic therapy on Candida glabrata biofilms formed in acrylic resin polymerized. Laser Med. Sci. 32 (3), 549–555. https://doi.org/10.1007/s10103-017-2147-4.

Hempstead, J., Jones, D.P., Ziouche, A., Cramer, G.M., Rizvi, I., Arnason, S., Hasan, T., Jonathan, P., Celli, J.P., 2015. Low-cost photodynamic therapy devices for global health settings: characterization of battery-powered LED performance and smartphone imaging in 3D tumor models. Sci. Rep. 5, 10093 https://doi.org/10.1038/srep10093.

Jiang, X., Fan, Z., Yu, Y., Shao, C., Suo, Y., Wei, X., Zhou, Y., 2015. Toluidine blue O and porphyrin-mediated photodynamic therapy on three main pathogenic bacteria of periodontitis using portable LED phototherapy device. J. Innov. Opt. Health Sci. 8 (4), 1550017 https://doi.org/10.1142/S1793545815500170.

Kercher, E.M., Nath, S., Rizvi, I., Spring, B.Q., 2020. Cancer cell-targeted and activatable photoimmunotherapy spares T cells in a 3D coculture model. Photochem. Photobiol. 96, 295–300. https://doi.org/10.1111/php.13153.

Kim, M.M., Darafsheh, A., 2020. Light sources and dosimetry techniques for photodynamic therapy. Photochem. Photobiol. 96, 280–294. https://doi.org/10.1111/php.13219.

Kirino, I., Fujita, K., Sakanoue, K., Sugita, R., Yamagishi, K., Takeoka, S., Fujie, T., Uemoto, S., Morimoto, Y., 2020. Metronomic photodynamic therapy using an implantable LED device and orally administered 5-aminolevulinic acid. Sci. Rep. 10, 1–10. https://doi.org/10.1038/s41598-020-79067-7.

Klimenko, V.V., Knyazev, N.A., Moiseenko, F.V., Rusanov, A.A., Bogdanov, A.A., Dubina, M.V., 2016. Pulse mode of laser photodynamic treatment induced cell apoptosis. Photodiagnosis Photodyn. Ther. 13, 101–107. https://doi.org/10.1016/j.pdpdt.2016.01.003.

Kwiatkowski, S., Knap, B., Przystupski, D., Saczko, J., Kedzierska, E., Knap-Czop, K., Kotlińska, J., Michel, O., Kotowski, K., Kulbacka, J., 2018. Photodynamic therapy – mechanisms, photosensitizers, and combinations. Biomed. Pharmacother. 106, 1098–1107. https://doi.org/10.1016/j.biopha.2018.07.049.

Lin, H.P., Chen, H.M., Yu, C.H., Yang, H., Wang, Y.P., Chiang, C.P., 2010. Topical photodynamic therapy is very effective for oral verrucous hyperplasia and oral erythroleukoplakia. J. Oral Pathol. Med. 39 (8), 624–630. https://doi.org/10.1111/j.1600-0714.2010.00935.x.

Liu, H., Daly, L., Rudd, G., Khan, A.P., Mallidi, S., Liu, Y., Cuckov, F., Hasan, T., Celli, J. P., 2019. Development and evaluation of a low-cost, portable, LED-based device for PDT treatment of early-stage oral cancer in resource-limited settings. Laser Surg. Med. 51 (4), 345–351. https://doi.org/10.1111/j.1600-0714.2010.00935.x.

Ogawa, K., Kobuke, Y., 2008. Recent advances in two-photon photodynamic therapy. Anti Cancer Agents Med. Chem. 8 (3), 269–279. https://doi.org/10.2174/187152008783961860.

Pereira, D., Pinto, J.G., Sorge, C.D., Benedito, F.R., Khouri, S., Strixino, J.F., 2013. Study of photodynamic therapy in the control of isolated microorganisms from infected wounds—an in vitro study. Laser Med. Sci. 29 (1), 113–120. https://doi.org/10.1007/s10103-013-1283-8.

Robertson, C.A., Evans, D.H., Abrahamse, H., 2009. Photodynamic therapy (PDT): a short review on cellular mechanisms and cancer research applications for PDT. J. Photochem. Photobiol. B Biol. 96 (1), 1–8. https://doi.org/10.1016/j.jphotobiol.2009.04.001.

Sailapu, S.K., Dutta, D., Simon, A.T., Ghosh, S.S., Chattopadhyay, A., 2019. Smartphone controlled interactive portable device for theranostics in vitro. Biosens. Bioelectron. 146, 111745 https://doi.org/10.1016/j.bios.2019.111745.

Turna, O., Baykal, A., Kucukkara, E.S., Ozten, O., Ozkan, A.D., Eskiler, G.G., Kamanli, A. F., Bilir, C., Yildiz, S.Z., Kaleli, S., Ucmak, M., Kasikci, G., Lim, H.S., 2022. Efficacy of 5-aminolevulinic acid-based photodynamic therapy in different subtypes of canine mammary gland cancer cells. Laser Med. Sci. 37 (2), 867–876. https://doi.org/10.1007/s10103-021-03324-y.

Yanovsky, R.L., Bartenstein, D.W., Rogers, G.S., Isakoff, S.J., Chen, S.T., 2019. Photodynamic therapy for solid tumors: a review of the literature. Photodermatol. Photoimmunol. Photomed. 35, 295–303. https://doi.org/10.1111/phpp.12489.

Yoon, I., Li, J.Z., Shim, Y.K., 2013. Advance in Photosensitizers and light delivery for photodynamic therapy. Clin. Endosc. 46 (1), 7–23. https://doi.org/10.5946/ce.2013.46.1.7.

Yu, C.H., Lin, H.P., Chen, H.M., Yang, H., Wang, Y.P., Chiang, C.P., 2009. Comparison of clinical outcomes of oral erythroleukoplakia treated with photodynamic therapy using either light-emitting diode or laser light. Laser Surg. Med. 41 (9), 628–633. https://doi.org/10.1002/lsm.20841.

Yuzhakova, D.V., Shirmanova, M.V., Klimenko, V.V., Lukina, M.M., Gavrina, A.I., Komarova, A.D., Gorbachev, D.A., Sapogova, N.V., Lukyanov, K.A., Kamensky, V.A., 2021. PDT with genetically encoded photosensitizer miniSOG on a tumor spheroid model: a comparative study of continuous-wave and pulsed irradiation. Biochim. Biophys. Acta Gen. Subj. 1865 (12), 129978 https://doi.org/10.1016/j.bbagen.2021.129978.

Zeitouni, N.C., Sunar, U., Rohrbach, D.J., Paquette, A.D., Bellnier, D.A., Shi, Y., Wilding, G., Foster, T.H., Henderson, B.W., 2014. A prospective study of pain control by a 2-step irradiance schedule during topical photodynamic therapy of nonmelanoma skin cancer. Dermatol. Surg. 40 (12), 1390–1394. https://doi.org/10.1097/DSS.0000000000000183.

Zhang, K., Timilsina, S., Waguespack, M., Kercher, E.M., Spring, B.Q., 2022. Photodynamic therapy experiments. Sci. Rep. 12, 19341 https://doi.org/10.1038/s41598-022-22020-7.

Zhang, Y., Jiang, S., Chen, H., Zou, X., 2017. Hemoporfin-mediated photodynamic therapy for the treatment of port-wine stain birthmarks in pediatric patients. An. Bras. Dermatol. 92 (4), 559–561. https://doi.org/10.1590/abd1806-4841.20176431.